Observability analysis and optimization of autonomous orbit determination through relative sensing

Pedro Rocha Cachim
pedrocachim@tecnico.ulisboa.pt

Instituto Superior Técnico, Universidade de Lisboa, Portugal

October 2020

Abstract

Within the context of spacecraft formation flying localization methods, autonomous orbit determination through relative sensing is one of the most promising concepts discussed in the literature. Despite its potential, it is yet to be implemented in practice. In this thesis, the SunRISE mission concept will be used as a case study to explore the potential of this method. After comparing it with the mission's previously proposed localization methods, an optimization study will be made to place a new satellite in the formation so as to maximize its localization accuracy. Finally, a new study will be done on the possibility of removing the relative bearing measurement systems from the spacecraft in the formation while maintaining the observability of their position in the inertial frame, and the resulting performance will be evaluated and compared with the previous results.
Keywords: Spacecraft formation flying, relative positioning, trajectory optimization, observability study

1. Introduction

Over the last few decades, a great focus has been given to the goal of reducing the costs of space exploration missions. Among the new concepts and developments being studied for this purpose, formation flying may prove to be one of the most important technological shifts to influence the space industry. The interest in Flying Formations stems from the ability to divide the payload and operational functions of a spacecraft between several elements [1].

The fractioning of a single large satellite into several smaller ones should not only lead to a reduction in cost, but also to an increased reliability, since the loss of one element would not necessarily imply the collapse of the system [2]. Furthermore, FF can extend the realm of possible science missions that would otherwise be impractical with a single spacecraft [3]. Applications that require large and precise baseline separations such as interferometry and gravimetry could particularly benefit from the attributes of FF [1].

One of the most challenging aspects of spacecraft FF missions is the design of on-board guidance, navigation and control (GNC) techniques [4]. So far, the navigation solutions adopted by most FF missions have relied on GNSS receivers. Even the MMS mission, in which the formation reached orbital apogees extending as far as 25 Earth radii, opted to use a GPS receiver tuned to acquire low strength GPS signals to allow for positioning at high altitudes [5]. In deep space missions, orbit determination systems are tipically dependent on ground station telemetry [6].

However, ground station telemetry in deep space missions does not allow for knowledge of the real-time state due to the time delay. For certain missions, such as those that involve the landing of equipment on a planet's surface, that time delay becomes a considerable predicament [7]. Overcoming this challenge will require autonomous, real-time navigation methods.

Seeking to find a solution to the previous problem, Markley demonstrated that the time history of the relative positioning of the spacecraft in a formation can allow for the observation of their absolute position in an inertial frame [8]. This method has been extensively researched since, as it provides an autonomous and real-time means of observing the absolute position, regardless of the distance or visibility to the ground stations or GNSS constellation.

In order to contribute to the research on the relative positioning autonomous navigation method, a case study will be necessary. Due to the sparseness of deep-space flying formation concepts, however, the Earth-centered SunRISE mission concept was selected [9]. A study done on potential navigation methods to achieve SunRISE's positioning

requirements compared a relative positioning-only method with a GNSS-based method [10]. Even though the study concluded that the latter was the better choice, their proposed relative positioning-only method did not make use of absolute state observability for autonomous navigation.

Using this concept as a template, 3 topics of discussion were set for this study:

- Analysis and comparison of a new relative positioning autonomous navigation method with the previously proposed navigation solutions for the SunRISE concept;
- Placement of an additional spacecraft in the formation in a configuration that optimizes the autonomous navigation system's performance;
- Possible suppression of system sensors while maintaining full state observability.

1.1. Related work

In this section, previous work by other researchers relevant to the topics mentioned above will be reviewed.

1.1.1 Autonomous navigation method

As mentioned before, the concept of using relative positioning within a multi-satellite mission for autonomous navigation was first suggested by Markley [8]. In his paper, Markley demonstrated the full observability of a positioning system with two spacecraft in keplerian orbits around the same body, and with relative position measurements (with orientation knowledge in an inertial frame) using the observability matrix. Markley also reached the conclusion that this system will become unobservable if both spacecraft always have the same altitude, and are either coplanar or oriented such that they cross the line of intersection of the two orbital planes simultaneously.

Further studies have been done on the observability of this system. Psiaki first proposed a batch filter to autonomously determine the orbits of 2 spacecraft based on measurements of the relative position vector from one spacecraft to the other [11]. Later on, Psiaki further developed this method so that it could also autonomously determine positions while allowing for corrections of the gravity model of the celestial body around which the spacecraft orbit [12].

1.1.2 Observability Optimization

Within the topic of absolute positioning through relative positioning measurements, the question of which orbital configuration will optimize the accuracy of the system has already been addressed in the literature. Ou studied the impact of the formation's absolute orbital elements on the observability within a 2-element formation [13]. A subsequent study concentrated in designing an autonomous navigation scheme for Mars exploration [14].

1.1.3 System Sensor Reduction

Since relative positioning systems that do not depend on tracking systems estimate the relative position through separate measurements of the range and LOS (Line-Of-Sight) vector, studies have also been done on the observability of a system with ranging-only [15] and LOS vector-only [16].

According to Yim's work [16], relative LOS vector measurements with inertial attitude information allow for the system to be observable, even without J_2 perturbations from the Earth's oblateness effect on its gravity field. This system is only unobservable when the two spacecraft are in the same orbiting plane with no inclination. Increasing the complexity of the gravity field of the central body or the overall inclination of the formation may increase the system's observability.

Hill found that ranging measurements in the two-body problem could observe the shape, phase and relative orientation of the orbits of the two spacecraft, but not the absolute orientation with respect to the inertial frame of reference, due to the spherical symmetry of the two-body problem's gravity field model [15]. The problem can become observable when the asymmetries of the central body's gravity field are considered [15, 17]. Another way to render this system observable through ranging measurements is to consider three-body problem dynamics, in which one of the spacecraft is in the Lagrange points 1 or 2. This concept of navigation for the Earth-Moon system is known as LiAISON [18], and has been proposed as a method of autonomous navigation for vehicles on the far side of the lunar surface.

2. Localization methods

The SunRISE mission, proposed by NASA's Jet Propulsion Laboratory, aims at studying the acceleration of solar energetic particles at Coronal Mass Ejections. The mission consists of a spacecraft formation with 6 identical 6U CubeSat forming an observatory in a 25-hour circular orbit slightly above GEO. The spacecraft's formation is kept passively, with interspacecraft distances ranging from $\sim 1-10$ km along an orbit. In order to achieve its scientific objectives, the mission requires a maximum 3 m relative positioning accuracy.

Two solutions were discussed in [10] for the positioning system of the SunRISE mission: a GNSS-based method, and a RF/vision-based method. De-

spite the study's conclusion that the former was the better solution, it also concluded that the latter had potential room for improvement. We will therefore make a description of the RF/vision-based method, followed by a proposed alternative filtering solution.

2.1. RF/vision-based method

The alternative proposed method to achieve the relative positioning accuracy requirement is based on range and bearing measurements between the spacecraft. Each spacecraft carries a UHF radio to perform relative ranging, and a star tracker/camera that can measure the orientation of another spacecraft with respect to an inertial frame of reference.

2.1.1 Crosslink schedule

This method is built on the assumption that relative measurements between spacecraft can only be performed in pairs, and therefore a measurement schedule is necessary such that every spacecraft gets the chance to perform one set of measurements with every other spacecraft within a measurement cycle. The proposed measurement schedule is shown in Table 1, in which the spacecraft are identified with indexes from 1 to 6. For each measurement set, relative range and bearing observations between pairs are made every second. The time between sets accounts for the time required for the spacecraft to slew and point the cameras towards each other and for the radios to lock onto each other.

Time Interval, min	S/C Pairs		
$[t_0 + 9 + 50k, t_0 + 10 + 50k]$	**1-2**	**3-4**	**5-6**
$[t_0 + 19 + 50k, t_0 + 20 + 50k]$	**1-3**	**2-5**	**4-6**
$[t_0 + 29 + 50k, t_0 + 30 + 50k]$	**1-4**	**2-6**	**3-5**
$[t_0 + 39 + 50k, t_0 + 40 + 50k]$	**1-5**	**2-4**	**3-6**
$[t_0 + 49 + 50k, t_0 + 50 + 50k]$	**1-6**	**2-3**	**4-5**

Table 1: Measurement schedule, where t_0 is the starting epoch and $k \in \mathbb{Z}^+$ [10]

2.1.2 Extended Kalman Filter

The filtering algorithm proposed in [10] for this positioning system consists of a simple EKF. The objective of the EKF is to obtain an estimate of the system state $x \in \mathcal{R}^p$ modelled after a dynamic system $\dot{x}(t) = f(x(t), t, w)$ with observation equations $y(t) = h(x(t), t, \nu)$, where $y \in \mathcal{R}^m$ denotes the available observations on the system's states, $w \in \mathcal{R}^p$ represents process noise to account for modelling innaccuracies and $\nu \in \mathcal{R}^m$ represents measurement noise. Kalman Filters are built on the assumption that noise can be modelled as centered white noise, meaning that $w \sim \mathcal{N}(0, Q)$ and $\nu \sim \mathcal{N}(0, R)$.

Prediction model

The Extended Kalman Filter proposed in [10] follows a PVA (Position-Velocity-Acceleration) model, meaning that its state vector accounts for the position, velocity and acceleration of each of the elements within the formation.

Let us consider $\delta r_{j/1}$ the position vector of spacecraft $j \in [2, ..., 6]$ with respect to spacecraft 1 in an inertial frame centered at the latter. Its corresponding velocity vector in the same frame of reference is $\delta v_{j/1}$, and its acceleration vector is $\delta a_{j/1}$. In matricial form, the continuous-time propagation of these states in the PVA model is

$$\dot{x}_j = A_j x_j + G_j w_j \Leftrightarrow$$
$$\begin{bmatrix} \dot{\delta r}_{j/1} \\ \dot{\delta v}_{j/1} \\ \dot{\delta a}_{j/1} \end{bmatrix} = \begin{bmatrix} \mathbf{0} & I & \mathbf{0} \\ \mathbf{0} & \mathbf{0} & I \\ \mathbf{0} & \mathbf{0} & \mathbf{0} \end{bmatrix} \begin{bmatrix} \delta r_{j/1} \\ \delta v_{j/1} \\ \delta a_{j/1} \end{bmatrix} + \begin{bmatrix} \mathbf{0} \\ \mathbf{0} \\ I \end{bmatrix} \begin{bmatrix} w_{j_1} \\ w_{j_2} \\ w_{j_3} \end{bmatrix} \quad (1)$$

where w_j is a centered Gaussian white noise process with covariance $E\{w_j(t)w_j^T(\tau)\} = Q\delta(t - \tau) = q_j I\delta(t - \tau)$, and in [10] q_j was set to $(1\text{e}{-7})^2(\text{m/s}^3)^2 \forall j \in \{2, \ldots, 6\}$. The full state vector x for the formation is a direct sum of the individual propagation system of each relative spacecraft motion state vector x_j for $j \in \{2, \ldots, 6\}$. The complete full state dynamic model is therefore

$$\dot{x} = Ax + Gw, \quad (2)$$

where $A = \text{diag}(A_2, \ldots, A_6)$, $G = \text{diag}(G_2, \ldots, G_6)$, $x = \{x_j\}$ and w is the concatenation of the white noise processes w_j, akin to that of the full state vector. The full process covariance matrix Q is similarly the direct sum of all $Q_j, \forall j \in \{2, \ldots, 6\}$.

Observation model

According to the measurement schedule in Table 1, measurements will be made between any pair of two spacecraft indexed j and n. The range and bearing measurements within a pair describe the relative position vector in the inertial frame from one spacecraft to the other, $\delta r_{j/n} = [\delta r_{x,j/n}\ \delta r_{y,j/n}\ \delta r_{z,j/n}]^T$. Relative positions between a pair that does not include the chief spacecraft (indexed 1) can be decomposed into relative position vectors that belong to the state vector x as

$$\delta r_{j/n}(t) = \delta r_{j/1}(t) - \delta r_{n/1}(t), \forall j \neq n \in \{2, ..., 6\}. \quad (3)$$

Range and bearing (expressed through right ascendancy and declination angles) of spacecraft j from

spacecraft n are expressed as

$$\rho_{j/n}(t) = \left\|\delta r_{j/n}(t)\right\| + \nu_\rho(t) \tag{4}$$

$$\psi_{j/n}(t) = \arctan\left(\frac{\delta r_{y,j/n}(t)}{\delta r_{x,j/n}(t}\right) + \nu_\psi(t) \tag{5}$$

$$\theta_{j/n}(t) = \arcsin\left(\frac{\delta r_{z,j/n}(t)}{\left\|\delta r_{j/n}(t)\right\|}\right) + \nu_\theta(t) \tag{6}$$

where $\nu_\rho(t)$, ν_ψ and ν_θ are Gaussian white noise process with covariances set in [10] as $E\{\nu_\rho(t)\nu_\rho(\tau)\} = (1/3)^2\delta(t-\tau)\mathrm{m}^2$ and $E\{\nu_\psi(t)\nu_\psi(\tau)\} = E\{\nu_\theta(t)\nu_\theta(\tau)\} = (35)^2\delta(t-\tau)\mathrm{arcsec}^2$. These are incorporated into the diagonal entries of the measurement noise covariance matrix R.

2.2. Proposed solution

In the new proposed version of the filter, the state vector and prediction model are modified. Whereas the previously proposed state vector incorporated the position, velocity and acceleration vectors in an inertial frame centered at an arbitrary spacecraft, we now propose to remove the relative acceleration vector states for each of the spacecraft, and to add the absolute position and velocity vectors of the chief spacecraft 1 in the ECI frame.

By including the absolute position into the state vector, the two-body problem dynamic model can be incorporated into the EKF. The propagation of the absolute position is done with the following set of equations:

$$\begin{cases} \dot{r}_1 &= v_1 \\ \dot{v}_1 &= -\mu\dfrac{r_1}{\|r_1\|^3} + \omega_1 \end{cases}. \tag{7}$$

The relative states of spacecraft j with respect to the chief spacecraft 1 in a local inertial frame centered on the latter, in turn, are propagated according to the following set of equations:

$$\begin{cases} \dot{\delta r}_{j/1} &= \delta v_{j/1} \\ \dot{\delta v}_{j/1} &= -\mu_\oplus\left(\dfrac{r_1+\delta r_{j/1}}{\|r_1+\delta r_{j/1}\|^3} - \dfrac{r_1}{\|r_1\|^3}\right) + \omega_j \end{cases}. \tag{8}$$

These equations are discretised and computed numerically using *MATLAB*'s *ode45* with the default relative and absolute tolerance of 1e−3 and 1e−6, respectively. The STM (State Transition Matrix) is also propagated through this method and used for the term Φ_k in the EKF equations. The process noise are modelled similarly to the previous filter, with the exception that $q_1 = (1\text{–}6)^2(\mathrm{km/s^2})^2$ and the remaining q_j are set to $(1\text{–}9)^2(\mathrm{km/s^2})^2$.

2.3. Filter comparison

In this section, Monte Carlo simulations will be run ($M = 40$ samples) in order to compare the two configurations of the EKF and their performance in terms of accuracy.

The trajectory generation approach in [10] consisted only of a two-body dynamic model with an added constant acceleration in an arbitrary direction representing non-keplerian perturbations. Since the study [10] focuses exclusively on relative positioning and does not account for orbit dynamics in its filter prediction step, the simulation period can be reduced to a portion of an orbital period. However, in the present study we intend to propose an improved filter that includes the estimation of the absolute position. The new filtering technique is therefore tested with a simulation period extending to one orbital period, and with as accurate a real trajectory as possible. In this study, the simulation's real trajectory incorporates solar radiation pressure, gravitational pull from the Sun and Moon and an Earth gravity geopotential model included in the *ODTBX* Toolbox.

In [10], an error of 100 m and 1 cm/s in a random direction was given to the initial relative position and velocity vector state estimates $\hat{\delta r}_{j/1}(t_0)$ and $\hat{\delta v}_{j/1}(t_0)$, respectively, while the initial accelerations were assumed to be zero. The corresponding diagonal entries of the initial state covariance matrix are the squared value of that same initial error ($(0.01\,\mathrm{km}^2$ for position entries and $1\times10^{-10}\,(\mathrm{km/s})^2$ for velocity entries), with the exception of the acceleration entries being set to $1\times10^{-14}\,(\mathrm{km/s^2})^2$. Save for the acceleration entries, these initialization parameters also apply to the new filter's simulation.

In table 2 the RMS error values of the original and proposed filter are compared. The results of the PVA EKF are shown for both the simulation method described in [10] and for the new approach in this study. The RMS values only account for the period after which the filters have converged (~ 200 min). The mean relative position error is the average of the RMS position error of the deputy spacecraft with respect to the chief spacecraft. The absolute position error corresponds to the RMS error of the absolute position of the chief spacecraft.

	Abs. pos. error (km)	**Mean rel. pos. error (m)**
PVA EKF (results in[10])	-	3.6
PVA EKF new simulation	-	3.6
Added absolute states EKF	1.82	0.13

Table 2: RF/vision filter RMS error comparison.

The new simulation conditions provide very close results to those obtained in [10]. The difference in error between the original and the proposed solu-

tion in the new simulation environment shows that the addition of the absolute position and keplerian dynamics to the filter significantly improves the accuracy of the algorithm (by a factor of ~ 30).

The proposed modifications to the RF/vision-based navigation solution seem to improve the overall performance of the system, not only increasing the relative positioning accuracy, but also by allowing the formation to autonomously determine its absolute position. However, the absolute positioning accuracy of this method underperforms that of the chosen GNSS-based navigation solution for the mission by a factor of ~ 1000.

3. Observability Optimization

As suggested in the first study that proposed the concept of autonomous navigation through the observation of the time history of the relative position of spacecraft in an inertial frame [8], the observability of the system is heavily dependent on the orbital configuration of the spacecraft performing the measurements. In order to further explore the potential of this method, this study will focus on adding a new spacecraft to the case study formation, such that its orbital configuration optimizes the navigation system's performance.

The generic mathematical formulation for the problem in question is described as

$$\begin{aligned} \underset{x\in\mathcal{D}}{\text{minimize}} \quad & f(x) \\ \text{subject to} \quad & f_i(x) \leq 0,\ i \in \{1,...,m\} \\ & h_j(x) = 0,\ j \in \{1,...,p\} \end{aligned}$$

where x describes the initial orbital configuration of the new spacecraft, $f(x)$ is the objective function that quantifies the observability/performance of the system, and $f_i(x)$ and h_j are the inequality and equality constraints, respectively.

3.1. Objective function

Several choices exist regarding the choice of objective function for the problem in question. Two tools were used to evaluate and quantify the observability/performance of the dynamic system:

- The continuous-time *Observability matrix* $\mathcal{O}$ up to order 3 as described in [8]. Within the context of this study, it will be used to study which results would optimize local observability across the trajectory, in the absence of measurement noise;
- The inverse of the SFIM (*Standard Fisher Information Matrix*) serves as an estimate of the state covariance of a discrete-time nonlinear system [19]. For numerically more accurate results, the square-root of the SFIM (SR-SFIM) was used, calculated as $\mathcal{I} = [(R^{-1/2}H_0\Phi_{0|0})^T \ \dots \ (R^{-1/2}H_k\Phi_{k|0})^T]^T$.

2 metrics from each of these matrices were chosen for optimization: the smallest singular value and the condition number (ratio of largest to smallest singular value):

- Maximizing the smallest singular value (or minimizing its negative value, which will be referred to in this study as *Local Unobservability Index* or LUI) can be explained as increasing the observability of the least observable subspace in the context of the observability matrix, or decreasing its estimation error variance when considering the SR-SFIM;
- Minimizing the condition number (or its negative reciprocal value) should lead to a better conditioned matrix, decreasing the disparity in observability or estimation error between the least and most observable subspaces.

These metrics can be taken from any matrix and used to evaluate how close to singular it is. The observability matrix in question, however, only evaluates local observability within a given point in time. In order to evaluate the observability of a trajectory using the observability matrix, it was decided to average the corresponding metric across time steps. The SR-SFIM is calculated considering a set of observations from a given trajectory, and therefore can be used directly.

Relative Positioning System

Based on precedents established by previous missions and available current technology, 2 measurement systems were considered in this optimization problem:

- The RF/vision-based system described in Section 2.1 that was proposed for the case study formation, with equivalent error model;
- An RF-only system, that uses multiple receivers and TOA (Time-Of-Arrival) differencing to estimate the (AOA) Angle-Of-Arrival of the signal, which can be used with absolute orientation knowledge to estimate relative bearing.

Both models incorporate a Gaussian white noise model for the ranging and bearing observations. The values for the covariance of the RF/vision-based system have already been described in Section 2.1. For the RF-only system, the ranging accuracy will be similar, but the relative bearing will be more innacurate, with a standard deviation of 1° for the right ascension and declination angles (based on the accuracy presented by the FFRF system onboard the PRISMA mission [20]).

The lower accuracy presented by the RF-only system is compensated by the assumption that the system can perform measurements regardless of the distance between the spacecraft within the Earth's sphere of influence. The RF/vision-based system will present a maximum distance constraint to account for the camera's functional range.

Due to this constraint, the orbital period of any spacecraft employing this system must be similar to that of the chief spacecraft. The question of whether or not to apply the restriction of synchronizing the orbital motion of the new spacecraft with the formation led to the decision of studying 2 different configurations for the RF-only system:

- *Free-period configuration*: In this configuration, the new spacecraft has the freedom to have a different orbital period than that of the formation, which equates to a_2 being a part of the variables x. This configuration incurs the problem that the orbits will become asynchronous, making it difficult to evaluate how the system will perform over time;
- *Fixed-period configuration*: The semi-major axis a_2 is set equal to that of the formation a_1, synchronizing the orbits and making the relative orbital motion periodic. The periodicity of the motion makes the filtering simulation results of one orbital period more descriptive of its overall behaviour.

For the SR-SFIM RF-only free-period and the observability matrix configurations, the objective function is calculated for the duration of the orbit with the longest orbital period between the chief and the new spacecraft. Because the SR-SFIM cost functions benefit from considering a greater number of observations, a period factor $f_{\text{period}} = T_1/\max(T_1, T_2)$ is multiplied to the objective function of the RF-only free-period configurations.

Dynamic system approximations

In order to reduce the computation time of each $f(x)$ evaluation, the dynamic system was reduced to a 2 spacecraft system, with one spacecraft being the chief orbit used to design the formation (indexed 1) and the other being the new spacecraft. Additionally, the sampling period was changed from the previously mentioned schedule to a fixed constant sampling period of $90s$.

Eclipse condition

Within a configuration in which the new spacecraft has a wider search space available, it is possible for the Earth to obstruct the field-of-view between it and the formation. This obstruction should be accounted for in the objective function, such that measurements become unavailable during the "eclipse" period. In this period, the LUI and the negative reciprocal of the CN are set to zero.

The SR-SFIM-related cost functions are multiplied by the ratio of uneclipsed per total observations used in the functions calculation to further discourage the presence of occultation periods in these results.

3.2. Constraints and Search Domain

The variables to be optimized x describe the initial state of the new spacecraft. The Classical Orbital Elements are generically used ($x = \{a_2, e_2, i_2, \Omega_2, \omega_2, \nu_2\}$, where a is the SMA, e is the eccentricity, i the inclination, Ω the RAAN, ω the argument of the perigee and ν the true anomaly).

Restrictions need to be applied to the domain of x, however. The perigee of the orbit must stay above a given threshold to avoid excessive atmospheric drag (defined at 6678 km) and the apogee must stay below 3×10^5 km, to place a ceiling on the computation time of the objective function (which is proportional to the duration of the longest orbital period of the two spacecraft). For the configurations of the optimization problem that restrict the new spacecraft's orbital period (and therefore semi-major axis $a_2 = a_1 = a$),these restrictions limit the eccentricity such that $e_2 \in [0, 0.85]$.

For the free orbital period configurations, in order to avoid nonlinear constraints, the elements a_2 and e_2 are replaced with the radius of the orbit at the apsides $r_1, r_2 \in [R_{min}, R_{max}]$. a_2 and e_2 are then calculated from these elements according to $a_2 = (r_1 + r_2)/2$ and $e_2 = |r_1 - r_2|/(r_1 + r_2)$.

The functional range restriction for the vision-based system, however, requires a nonlinear constraint. Setting this distance as $d_{max} = 480$ km (based on the PRISMA mission's VBS system with a 20 km margin), it is not easy to apply this restriction on the initial states of the formation. In order to do so, relative motion was modelled by the approximated equations in the LVLH frame derived from the Hill-Clohessy-Wiltshire equations. The maximum distance constraint between the spacecraft is expressed as

$$a[(|\omega_2 + M_2 + \Omega_2 - \omega_1 - M_1 - \Omega_1| + 2e_2)^2 + (i_2 - i_1)^2]^{1/2} - d_{max} < 0 \quad (9)$$

with M the mean anomaly, which can be obtained from the true anomaly ν and eccentricity e. This formulation was based on the considerations that the chief orbit is near-circular and near-equatorial, and that both spacecraft have an equal orbital period.

	$a(km)$	e	$i(rad)$	$\Omega(rad)$	$\omega(rad)$	$\nu(rad)$
chief orbit	43399	0	0	0	0	0
LUI-opt. S/C	6678	0	1.54	2.25	6.13	2.12
CN-opt. S/C	6678	0	1.51	4.9e−03	2.92	1.40

Table 3: Initial COE of the Observability Matrix-optimized new spacecraft.

3.3. Optimization Results

For the optimization problems with nonlinear constraints, *MATLAB*'s *fmincon*'s Interior Point Algorithm with multi-start was used as a global solver [21]. For the remaining ones, *PSwarm* was used [22]. Each algorithm is run for a period of $\sim$ 8 hours.

Observability Matrix

The observability-optimized orbital configurations for the new spacecraft are described in Table 3.

The optimized values of the objective function for each problem were near identical, at $\sim$ 9.91e−07. Upon closer inspection, it was observed that the relative state subspaces are always equally observable (the corresponding singular values are unitary), and therefore there is no difference between the reciprocal of the CN and the smallest singular value.

Between the two results, the only COE that converged to similar values are the semi-major axis a_{new} and the eccentricy e_{new}. The new S/C orbit also tends to become near polar ($i_{new} \sim 90°$), which might come as a result of minimizing eclipsed time.

These results give insight into which orbital configurations would optimize the observability of the system. In general, these results seem to indicate that large differences in magnitude of gravitational acceleration improve the local observability of the least observable (absolute) states.

SR-SFIM RF/vision system

We now evaluate the results of the optimization problems that use the CN and LUI of the SR-SFIM matrix, when considering the RF ranging and vision bearing measurement system for the new auxiliary spacecraft. The optimized orbits are shown in Figure 1 in the LVLH plane, since these are indiscernible in the ECI frame due to their close promixity to the chief spacecraft.

In these configurations, the differences in the results that come from optimizing either the condition number or the smallest singular value are more visible. Since the state error covariance of the relative states increases with the distance between the spacecraft, all singular values are affected by the orbital configuration, unlike with the observability matrix.

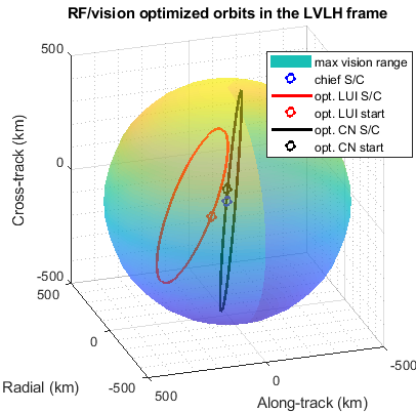

Figure 1: Optimized orbits for the RF/vision based system in the LVLH frame centered around the chief orbit.

The CN-optimized configuration leads to a new relative orbit with wider out-of-plane motion and closer in-plane motion when compared to the LUI-optimized configuration.

By performing singular value decomposition of the SR-SFIM matrix of the optimized results, we can use the right singular vectors to know which states the smallest and largest singular values are most associated with. In both configurations, the largest singular value is linked with δv_y, the Y component of the relative velocity of the new spacecraft with respect to the chief orbit in the ECI frame, while the smallest singular value corresponds most to r_y, the Y component of the chief spacecraft's absolute position vector in the ECI frame.

SR-SFIM RF-only system

In this section, we will evaluate the optimized orbital configurations for the SR-SFIM RF-only system. The results are shown in Figure 2.

The free-period configurations achieve only slightly better results than the fixed period results. Figure 2 also shows how close the free and fixed period CN-optimized new orbits are to each other with respect to the eccentricity, inclination and orbital plane orientation. The free and fixed period LUI-optimized orbits, despite only presenting a similarity in terms of eccentricity, achieve very close results.

None of the four optimized new orbits present Earth-eclipsed periods. Whereas the CN-optimized configurations are highly eccentric, the LUI-optimized orbits present a comparatively small degree of eccentricity ($e_2 \simeq 0.37$). All optimized orbits are near-polar ($i_2 \sim 90°$) with the exception of the fixed-period LUI-optimized one.

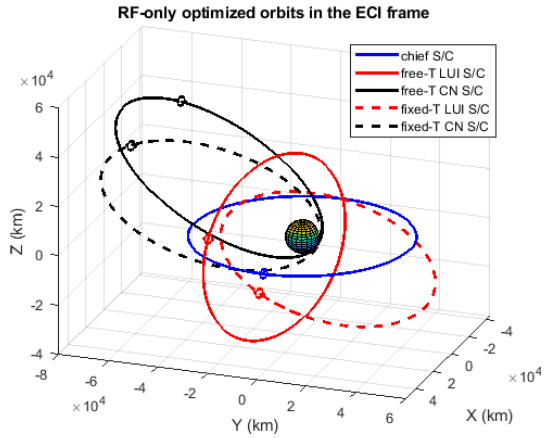

Figure 2: Optimized new spacecraft orbits for the RF-only system with free and fixed orbital period. The dots mark the initial S/C states.

4. System Sensor Reduction

As mentioned in Section 1.1.3, previous studies have demonstrated that, with keplerian motion, in a 2 spacecraft formation performing ranging-only measurements, 9 out of 12 position and velocity vector states can be observed at most. The unobservable subspace corresponds to the absolute orientation elements ω,Ω and i [15].

However, ranging history allows for the observation of relative orientation elements θ, ϕ_1 and ϕ_2. Of these, θ is the angle between the orbital planes, ϕ_1 is the angular distance along the orbit of spacecraft 1 from the periapsis to one of the two intersections of the orbits, and viceversa for ϕ_2 with respect to the orbit of the second spacecraft. These paraments are functions of the absolute orientation elements of both spacecraft. This implies that, with knowledge of one of the spacecraft's absolute orientation elements, the other one's absolute orientation elements could also be deduced.

The previous reasoning would imply that, within a formation with more than two spacecraft, if one pair is performing relative ranging and bearing measurements to observe their full state, then the remaining spacecraft only need to perform ranging measurements with either of these two in order for their position and velocity states to become observable.

4.1. Observability Analysis

In order to test the previous hypothesis, we consider a simplified system with 3 spacecraft. The corresponding state vector is composed of the position and velocity vector of the chief spacecraft in the ECI frame and the position and velocity vectors of the remaining spacecraft in a local inertial frame centered on the first spacecraft. The propagation model is similar to that described in (7) and (8). The spacecraft pair 1 and 2 perform ranging measurements, while the spacecraft pair 1 and 3 perform relative range and bearing measurements every $90s$. We describe the discrete-time dynamic observation system with the propagation model $x_k = \phi(x_{k-1})$ and observation model $y_k = h(x_k)$, where x_k and y_k denote the state and observation vectors at time t_k. Considering $\Phi_{k|0}$ to be the state transition matrix from states x_0 to x_k, and $H_k = \left.\frac{dh}{dx}\right|_{x_k}$ the observation matrix, we construct the discrete-time observability matrix as $\mathcal{O} = [H_0^T \ (H_1\Phi_{1|0})^T \ \dots \ (H_k\Phi_{k|0})^T]^T$, where the simulation period $t_k - t_0$ corresponds to one orbital period. The resulting matrix had full rank 18, albeit with a condition number of 5.55×10^9. This implies that the system, despite observable in theory, presents a large disparity in state subspace observability and is therefore ill-conditioned. Simulations will be used to better evaluate the performance of this type of system.

5. Simulation Results

We seek to evaluate the results from the optimized orbits in a simulation environment. However, in order to do so, a new measurement schedule with the added spacecraft needs to be designed.

Two sets of results were obtained with different measurement schedules: one in which the assumption is made that no spacecraft can measure its position with more than one other spacecraft simultaneously, and therefore an adapted schedule is created (shown in Table 4 and denoted as schedule 1); and the other in which the original schedule of the formation runs parallel to the measurements between the chief and the new spacecraft (shown in Table 1 and denoted as schedule 2).

Time Interval, min	S/C Pairs		
$[t_0 + 9 + 50k, t_0 + 10 + 50k]$	**1-2**	**3-4**	**5-6**
$[t_0 + 19 + 60k, t_0 + 20 + 60k]$	**1-3**	**2-4**	**5-7**
$[t_0 + 29 + 60k, t_0 + 30 + 60k]$	**1-4**	**2-7**	**3-6**
$[t_0 + 39 + 60k, t_0 + 40 + 60k]$	**1-5**	**2-6**	**3-7**
$[t_0 + 49 + 60k, t_0 + 50 + 60k]$	**1-6**	**2-5**	**4-7**
$[t_0 + 59 + 60k, t_0 + 60 + 60k]$	**1-7**	**3-5**	**4-6**

Table 4: Adapted measurement schedule, where t_0 is the starting epoch and $k \in \mathbb{Z}^+$

Finally, the latter schedule will be used to validate the hypothesis that the formation does not require relative bearing measurements between each other so long as the chief spacecraft's position is known from relative positioning measurements with the new spacecraft.

The simulations are run with the Monte-Carlo method, with $M = 40$ samples, in which the initial position state estimates will be placed 100 m away

			Abs. pos. error (km)	Mean form. rel. pos. error (m)	new S/C rel. pos. error (m)
RF/Vision		LUI	1.783	0.158	5.680
		CN	1.801	0.157	5.043
RF only	free period	LUI	2.310	0.159	6103
		CN	3.885	0.168	81043
	fixed period	LUI	2.286	0.159	2869
		CN	3.675	0.170	66161

Table 5: Mean absolute and relative error for the optimized orbital configurations with schedule 1.

			Abs. pos. error (km)	Mean form. rel. pos. error (m)	new S/C rel. pos. error (m)
RF/Vision		LUI	1.697	0.134	5.660
		CN	1.716	0.131	5.139
RF only	free period	LUI	2.126	0.133	14344
		CN	6.970	0.169	91828
	fixed period	LUI	1.971	0.134	7182
		CN	3.327	0.139	57122

Table 6: Mean absolute and relative error for the optimized orbital configurations with schedule 2.

from the real initial position in a random direction. The simulation period is kept at one orbital period of the original formation ($\sim$ 25 hours). For the sensor reduced simulations, however, half the Monte-Carlo simulations are run, each with twice the simulation period, due to the filter's longer relative positioning error convergence time ($\sim$ 1000 min). The remaining aspects of the simulations were kept similar to those in Section 2.3.

5.1. Optimization Results

Tables 5 and 6 show the RMS error values obtained for each of the optimized configurations with schedules 1 and 2, respectively.

The results indicate that only the RF/Vision configurations for the auxiliary spacecraft matching or slightly improving the absolute positioning accuracy of the formation.

When comparing the results from both schedules, it is possible to note that schedule 2 generally provides better relative positioning accuracy within the original formation. The RF/vision-based system generally outperforms the RF-only system in absolute positioning performance, as well as relative positioning performance for the new spacecraft. The LUI-optimized configurations generally have better absolute positioning performance than the CN-optimized ones.

The large errors observed in the RF-only CN-optimized configurations appear to be linked to factors that are unaccounted for in the SR-SFIM-based cost functions, such as inconstant levels of process noise and the validity of the EKF's linearization approach.

5.2. Reduced System results

By removing the relative bearing measurements between spacecraft in the original formation, but keeping them for the measurements between the chief spacecraft and the new spacecraft with schedule 2, the results shown in Table 7 are obtained.

			Abs. pos. error (km)	Mean form. rel. pos. error (m)	new S/C rel. pos. error (m)
RF/Vision		LUI	3.070	0.8802	4.439
		CN	3.599	0.9164	3.253
RF only	free period	LUI	3.376	0.9465	3060
		CN	12.610	2.438	79303
	fixed period	LUI	7.353	1.532	7723
		CN	34.243	6.286	158028

Table 7: Mean absolute and relative error for the optimized orbital configurations with the sensor-reduced system.

The removal of the relative bearing measurements within the original formation leads to a decrease in relative and absolute positioning accuracy. The results show the LUI-optimized configurations outperforming the accuracy of their CN-optimized counterparts in terms of absolute positioning accuracy.

The time frame under which these results were produced made it unclear whether the positioning error was converging or not. After running new longer simulations (5 orbital periods) for each configuration, it became more evident that the error was slowly diverging, indicating that the system is too ill-conditioned for the EKF to converge.

6. Conclusions

Using the SunRISE mission as a case study, the results in Section 2 demonstrated that including the absolute position states and two-body dynamics into the filter results in better relative positioning accuracy than the PVA model initially proposed in [10] (13 cm as opposed to 3.6 m mean RMS relative positioning error). The new filter, however, has the disadvantage of requiring an initial absolute position estimate. Compared with the performance of the chosen GNSS-based solution, its absolute positioning RMS performance is worse by a factor of around $\sim$ 1000, while its relative positioning RMS performance is better by a factor of $\sim$ 10.

Regarding the observability optimization study, the following conclusions were drawn:

- The use of the continuous-time observability matrix leads to optimized configurations in line with the results shown in [13, 14], indicating that larger differences in magnitude of gravity acceleration between spacecraft lead to better local observability of the absolute position;

- The comparison of results between the original formation's capacity to perform autonomous navigation with and without the added spacecraft shows that in most configurations the new spacecraft worsens the absolute positioning accuracy of the original formation;

- The choice of objective function may not have been sufficiently adequate for this study for several reasons, such as: 1. approximating the formation to a single spacecraft; 2. not accounting for the measurement schedule; 3. the choice of the SFIM, which more accurately describes the performance of a nonlinear WLS filter than that of the implemented EKF;

- LUI-optimization generally provided more accurate absolute positioning results than the CN-optimization;

- The RF/vision based system provided more accurate absolute positioning than the RF-only system;

- The restriction of the orbital period of the new spacecraft to that of the original formation generally improved the positioning performance of the system, contrary to the expectations set by the optimization results.

Finally, regarding the study on the observability and performance of the formation when deprived of part of its relative bearing measurements, it was possible to conclude that 1. the observability study demonstrated that only one pair of S/C in the FF needs to perform relative bearing measurements for the system to remain observable, albeit ill-conditioned; 2. the removal of most of the relative bearing measurements from the system leads to the EKF diverging, likely due to the system's ill-conditioning.

6.1. Future Work

The following suggestions are left for a potential continuation of the line of work discussed here: 1. alternative objective functions should be considered for the new spacecraft configuration optimization problem (such as the PFIM [19], which could more accurately reflect the performance of the EKF in question); 2. new approaches to reducing the complexity of the computation of the objective function while maintaining the validity of the problem; 3. testing whether the sensor-reduced system positioning error would converge under a square-root filter better suited for ill-conditioned problems.

References

[1] Cory T. Fraser. *Adaptive Extended Kalman Filtering Strategies for Autonomous Relative Navigation of Formation Flying Spacecraft*. PhD thesis, Carleton University, 2019.

[2] G. Liu and S. Zhang. A survey on formation control of small satellites. *Proceedings of the IEEE*, 2018.

[3] S. Nag et al. Effect of satellite formations and imaging modes on global albedo estimation. *Acta Astronautica*, 2016.

[4] G Di Mauro, M Lawn, et al. Survey on guidance navigation and control requirements for spacecraft formation-flying missions. *Journal of Guidance, Control, and Dynamics*, 2018.

[5] L. Winternitz, B. Bamford, et al. GPS Navigation Above 76,000 km for the MMS Mission. In *39th Annual AAS Guidance, Navigation and Control Conference*, 2016.

[6] Oliver Montenbruck and Eberhard Gill. *Satellite Orbits: Models, Methods, and Applications*. Springer Science & Business Media, 2000.

[7] Soumyo Dutta and Robert D Braun. Statistical entry, descent, and landing performance reconstruction of the mars science laboratory. *Journal of Spacecraft and Rockets*, 2014.

[8] Landis Markley. Autonomous navigation using landmark and intersatellite data. In *Astrodynamics conference*, 1984.

[9] Farah Alibay, Justin C Kasper, T Joseph W Lazio, and Tim Neilsen. Sun Radio Interferometer Space Experiment (SunRISE): Tracking particle acceleration and transport in the inner heliosphere. In *2017 IEEE Aerospace Conference*. IEEE, 2017.

[10] J. Stuart et al. Formation flying and position determination for a space-based interferometer in GEO graveyard orbit. In *2017 IEEE Aerospace Conference*. IEEE, 2017.

[11] Mark L. Psiaki. Autonomous orbit determination for two spacecraft from relative position measurements. *Journal of Guidance, Control, and Dynamics*, 1999.

[12] Mark L. Psiaki. Absolute orbit and gravity determination using relative position measurements between two satellites. *Journal of Guidance, Control, and Dynamics*, 2011.

[13] Y. Ou et al. Autonomous orbit determination and observability analysis for formation satellites. In *2016* 35^{th} *Chinese Control Conference (CCC)*. IEEE, 2016.

[14] Y. Ou et al. Observability-based mars autonomous navigation using formation flying spacecraft. *The Journal of Navigation*, 2018.

[15] K Hill and George H. Born. Autonomous interplanetary orbit determination using satellite-to-satellite tracking. *Journal of guidance, control, and dynamics*, 2007.

[16] Jo R. Yim et al. Autonomous orbit navigation of two spacecraft system using relative line of sight vector measurements. In *Proceedings of the AAS Space Flight Mechanics Meeting*, 2004.

[17] Keric A. Hill et al. Autonomous orbit determination from lunar halo orbits using crosslink range. *Journal of Spacecraft and Rockets*, 2008.

[18] K. Hill, George H. Born, et al. Linked, autonomous, interplanetary satellite orbit navigation (LiAISON) in lunar halo orbits. 2006.

[19] M. Rafieisakhaei et al. On the use of the observability gramian for partially observed robotic path planning problems. In *Proceedings of* 56^{th} *IEEE Conference on Decision and Control*, 2017.

[20] J. Harr et al. RF metrology validation and formation flying demonstration by small satellites–the CNES participation on the PRISMA mission. In *Proceedings of the 4S symposium small satellites, systems and services, ESA SP-625*, 2006.

[21] R. Byrd et al. A trust region method based on interior point techniques for nonlinear programming. *Mathematical programming*, 2000.

[22] I. Vaz and L. Vicente. A particle swarm pattern search method for bound constrained global optimization. *Journal of Global Optimization*, 2007.